Photocatalytic degradation of reactive blue 21 using Ag doped ZnO nanoparticles

A.A. El-Bindary [1*], A. Ismail [2], E.F. Eladl [2]

[1]Chemistry Department, Faculty of Science, University of Damietta, Damietta 34517, Egypt.
[2]Environmental Science Department, Faculty of Science, University of Port Said, Port Said, Egypt.

Abstract

Ag-doping onto ZnO, various mole % (1, 3, 5, 7 and 9) of silver has been investigated for the photoactivity of the doped material in reactive blue 21 (RB21) degradation. The enhancement of photocatalytic activity is due to the modification of ZnO with an appropriate amount of Ag can increase the separation efficiency of photogenerated electrons and holes in ZnO. The optical band gap of the samples was found to be 3.14 eV for Ag/ZnO (3%), which proves the change in the acceptor level induced by the Ag atoms. The photodegradation rate was determined for each experiment and the highest values were observed for Ag/ZnO (3%) suggesting that it absorbs large fraction of the UV spectrum and absorption of more light quanta. The mineralization of RB21 has been confirmed by Chemical Oxygen Demand measurements. Furthermore, the kinetics and scavengers of the reactive species during the degradation were also investigated. It was found that the degradation of RB21 fitted the first-order kinetics and OH$^•$ radicals were the main species. Formation of OH$^•$ free radicals during irradiation is ascertained by photoluminescence studies using terephthalic acid as probe molecule.

1. Introduction

Organic dyes and pigments are increasingly used in various applications which cause serious problems in our planet. A recent report indicates that the wastewater is contaminated with 10% to 20% from the global production of the organic dyes which represents about 0.7 million tons annually [1]. These dyes are usually consist of complex structures and difficult to decompose [2]. So that, the release of such polluted wastewater to the environment causes massive environmental issues and negative impacts on human health [3]. This lead the researcher to evaluate different methods for the treatment of colored wastewater such as advanced oxidation processes (AOPs) [2], biological methods [4], sonocatalyst processes [5,6], coagulation and flocculation [7], and using of natural or synthetic adsorbents [8,9]. It has been shown that the AOPs can be used to remove and decompose a vast range of organic dyes into safe and ecofriendly compounds [10–12]. Among the APOs, photocatalytic degradation methods proved a high efficacy in the degradation of the organic dyes that are resistant to the biological degradation [13].

The photocatalytic degradation technique depends on the absorption of high energy photons by a suitable photocatalyst that can promote electrons to the conduction band (CB) leaving holes in the valance band (VB). These photogenerated electron-hole pairs produces the hydroxyl radicals which are responsible for the dye degradation [14]. Different semiconducting materials such as TiO_2, $SrTiO_3$, ZnO, WO_3 and Fe2O3 were reported to be used as photocatalysts [15,16].

Zinc oxide (ZnO) is one of the most commonly used semiconducting materials as a photocatalyst for the degradation of organic dyes because of its wide band gap energy 3.37 eV, large exciton binding energy 60 meV, high chemical stability, harmless nature, low cost and high photosensitivity [17–19]. However, one of the demerits of ZnO as a photocatalyst is that the rate of the electron-hole recombination is very fast, which decrease the degradation efficacy [20]. Doping of ZnO with impurity atoms like that of the transition metals presents new

energy level where electrons are restricted in this new level overcoming the high rate of electron-hole recombination [21]. Several metals were used in order to enhance the efficacy of ZnO by doping as ZnO-Ce nanoparticles [22], ZnO-Pd nanoparticles [23], ZnO-Mn nanoparticles [24], ZnO-Al nanoparticles [25] and ZnO-Ag nanoparticles [26]. However, it should be noted that not all transition metals improve the efficacy where some of them decrease the efficacy because of the in the increase in electron-hole recombination [27].

In this paper, we prepared Ag-doped ZnO nanoparticles using a combination of chemical precipitation and sonochemical methods. After the characterization of the prepared photocatalysts, they used for the degradation of reactive blue 21 (RB21) dye in aqueous solution. A generalized mechanism of chemical reaction of RB21 dye on photocatalysis has also been reported.

2. **Material and Methods**
2.1. *Materials*

Zinc sulfate heptahydrate ($ZnSO_4.7H_2O$), sodiumborohydride ($NaBH_4$) and silver nitrate ($AgNO_3$) were supplied by Sigma-Aldrich and used as received. A commercial textile dye reactive blue 21 (RB21) was obtained from Cromatos SRL, Italy, and was used without any further purification. A stock solution of RB21 (1.0 g/L) was used, which could be diluted to the required concentration with deionized water in the experiment. All chemical reagents were of analytical grade and used without any further purification. Samples were then conserved in desiccators over anhydrous $CaCl_2$ for further use**.**

2.2. *Preparation of silver-doped ZnO nanoparticles (Ag/ZnO) with ultrasonic deposition method*

ZnO was prepared previously through co-precipitation-sonochemical processes using deionized water as solvent. By the ultrasonic, ZnO doped with metallic silver (Ag^0) was prepared [28] by reducing Ag^+ ions in silver nitrate to Ag^0 on ZnO surface using sodium borohydride as a reducing agent. Firstly, 1.0 g of the previously prepared ZnO was added to 100 mL of deionized water. Then, the calculated amount of $AgNO_3$ for doping was added to ZnO suspension, where the silver concentration was 1, 3, 5, 7 and 9% (molar ratio) *vs.* ZnO. After adding a known amount of sodium borohydride (0.1 g) as a reducing agent for the reduction of Ag^+ to Ag^0, the mixture was kept for 2 hr at 40 °C in an ultrasonic bath with continuous agitation by a mechanical stirrer. A gradual change in color from white to gray was obviously noticed. The light gray precipitate (Ag/ZnO) was washed by deionized water to eliminate un- or loosely-loaded Ag, was dried overnight at 100 °C in a hot-air oven and was ignited at calcination temperature of 400 °C for 4 hr. Finally, the ignited catalysts were ground in an agate mortar and pestle and stored in desiccator over anhydrous $CaCl_2$.

2.3. *Catalyst characterization*

FTIR examination was completed utilizing a JASCO-FT/IR-4100 spectrometer (Jasco, Easton, MD, USA): the finely pounded tests were incorporated into KBr plates before investigation in the wavenumber extend 400–4000 cm^{-1}. The surface morphology of the samples was inspected utilizing scanning electron microscope (SEM) analysis at accelerating voltages of 20 kV (JEOL-JSM-6510 LV). The elemental distribution of Ag/ZnO was analyzed using the energy-dispersive X-ray spectroscopy (EDX) and taken on a Leo1430VP microscope with operating voltage 5 kV. Structural variations of the as-prepared materials was investigated by X-ray diffraction (XRD) technique using a Shimadzu XRD-6000 diffractometer (Shimadzu Corporation, Tokyo, Japan) equipped with Cu Kα radiation ($\lambda = 1.54$ Å). The 2θ range was varied between 5–80° at a scanning rate of 0.02°. The crystal system, space group and lattice parameters values were considered and optimized using CRYSFIRE and CHEKCELL computer programs [29]. Absorbance measurements of samples were performed on UV-visible spectrophotometer (Perkin-Elmer AA800 spectrophotometer Model AAS) using 1.0 cm quartz cell. Also, Fluorescence Spectrometer (LUMINA, Thermo Scientific) was employed for fluorescence measurements of samples using 1.0 cm quartz cell. Ultrasonic apparatus, Delta 920 (220 V, 300 W, 28 KHz) was used. The isotherm of adsorption/desorption of N_2 on catalyst at 77 K was performed using a Quantachrome Touch Win Instruments version 1.11. Curves were analyzed by utilizing Brunauer-Emmett-Teller (BET) method (P/P$_o$ from 0.05 to 0.35) for specific area, t-plot method for external area, volume and area of micropores; and Barrett-Joyner-Halenda (BJH) method for diameter determination of mesopores. HANNA instrument pH meter (model 211) was used for pH modification. HANNA instrument Waste water behavior photometer (model HI 83214) was used for the measurement of chemical oxygen demand (COD).

2.4. *Determination of point of zero charge*

The point of zero charge (pH_{PZC}) was resolute by solid addition method [30]. A series of 50 mL (0.1 M) KNO_3 solutions were prepared and their pH values (pH_0) were attuned in the range of 1.0 to 12.0 by addition of

0.1 mol/L HCl and 0.1 mol/L NaOH. To each solution, 0.1 g of catalyst was added and the suspensions were disturbed using shaking water bath at 25 °C. The final pH values of the supernatant were determined (pH_f) after 48 h. The difference between initial (pH_0) and final (pH_f) values ($\Delta pH = pH_0 - pH_f$) (Y-axis) was plotted against the initial pH_0 (X-axis). The intersection of resulting curve yielded the pH_{PZC} where ΔpH = zero.

2.5. Photocatalytic dye degradation experiments

The experimental system for the photodeclorization of 100 mL (40 mg/L, pH = 7.0) aqueous solution RB21 containing 1.0 g/L of the photocatalyst was established in a reactor of a cylindrical Pyrex-glass cell (5 cm inside diameter and 10 cm height) [31]. The suspensions were illuminated under air condition with a medium pressure UV lamp (Philips) which was situated above the reactor (distance 20 cm). The photocatalytic examinations were done under UV irradiation at room temperature using UV lamp: E_{photon} (eV) 3.10–3.94 with λ_{max} (nm) 400–315. The dispersions were sampled out at the structured time intervals during the irradiation process. In order to make certain that adsorption equilibrium between the photocatalyst surface and the RB21 dye took place, the suspensions were magnetically stirred for 30 min (in the dark) before irradiation. Thus, the surface adsorption effect in the removal of RB21 is eradicated. The influence of the initial solution pH was evaluated at different pHs from 2 to 11 (adjusted by HCl (0.1 M) and NaOH (0.1 M)), while RB21 dye concentration was preset at 40 mg/L and 1.0 g/L for the photocatalyst. Photocatalyst dose was changed from 0.2 to 1.8 g/L, for 40 mg/L of RB21 solution, at pH of 7. Also, the effect of the RB21 dye concentration was assessed by varying its concentration from 10 mg/L to 80 mg/L, in the presence of 1.0 g/L of photocatalyst, at a fixed pH of 7. Each sample was withdrawn at a particular time interval and instantly centrifuged at 20,000 rpm for 5 min to remove any dispersed solid catalyst particles for analysis. Finally, the absorbance of RB21 in the supernatant liquid was measured by a UV–visible spectrophotometer, at the maximal absorption wavelength of RB21, λ_{max} = 625 nm. The photodegradation experiments for different Ag/ZnO concentrations (1, 3, 5, 7 and 9%) were performed at 40 mg/L dye concentration, 1.0 g/L catalyst concentration and at pH of 7, to choose one of them to study in details.

The degradation rate (D) of the dye was calculated using Eq. (1):

$$D \% = (A_0 - A_t / A_0) \times 100 \qquad (1)$$

Where A_0 represents the initial absorbance of RB21 solution (blank), and A_t is the absorbance after t minutes of irradiation/reaction. According to the Beer–Lambert's law, A_0 and A_t are directly proportional to C_0 and C_t, where C_0 and C_t are the concentrations of blank and sample at (t) time [31].

Chemical oxygen demand (COD) of samples before and after photodegradation experiments were measured at regular time intervals. According to the Langmuir–Hinshelwood model, the photodegradation process of pollutants follows the pseudo first-order kinetics, so the photodecolorization rate was studied using Eq. (2):

$$\ln (C_0/C_t) = \ln (A_0/A_t) = kt \qquad (2)$$

The optical properties of the photocatalysts were studied by UV-visible absorption spectroscopy at room temperature. The powder samples were dispersed in paraffin oil by sonication then the optical properties were studied at wavelength from 200 nm to 800 nm where paraffin oil was the reference medium.

The photodegradation rate constant k (min^{-1}) was calculated from the slope of the straight-line segment of the plot of $\ln(C_0/C_t)$ and the reaction time t as a function of the used experimental parameters.

3. Results and discussion

3.1. FTIR Analysis

Infrared measurements were performed in order to figure out the purity and nature of Ag/ZnO nanoparticles. Mainly, there are no noticeably differences between the FTIR of Ag/ZnO (3%) (Figure 1). The observed bands at 3440 and 1120 cm^{-1} may arise due to O-H stretching and deformation respectively which is assigned to the water adsorption on the metal surface (Figure 1) [32,33]. At 1625 cm^{-1}, a relatively less intense band represents the O-H stretching of the adsorbed water molecules. Experimentally, the vibrations of Ag/ZnO are in the range of 500–700 cm^{-1}. Bands around 600 cm^{-1} are related to the oxygen deficiency and/or oxygen vacancy deficiency complexes present in ZnO [34].

3.2. X-ray diffraction

The XRD analysis was appointed to recognize the phase structure and the purity of the photocatalysts. The XRD patterns of Ag doped ZnO sample (3%) is shown in Figure 2. the sample has the typical hexagonal wurtzite structure with lattice constant a = b = 3.249 Å and c = 5.205 Å (space group P63mc, JCPDS card no. 36-1451) [35]. No additional peaks due to impurities were detected which indicating the high purity of the prepared Ag/ZnO. The peaks at 2θ = 31.78, 34.44, 36.25, 47.57, 56.60, 62.87, 67.93, 69.05° can be attributed to (100), (002), (101), (012), (110), (013), (112), (201) planes for ZnO, respectively [36].
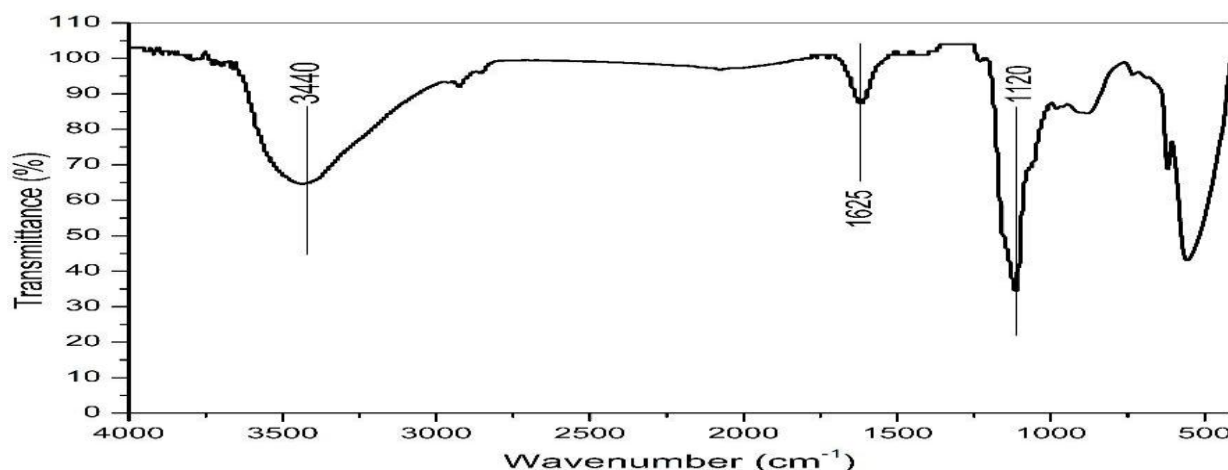
Figure 1: FTIR absorption peaks of Ag/ZnO (3%) photocatalyst.

Upon incorporation of metallic Ag on ZnO, three small extra diffraction peaks at $2\theta = 38.32$ and 44.58 and 63.70° were detected in the XRD pattern of Ag/ZnO (3%) that correspond to (111), (200) and (202) crystal planes of silver, respectively, confirming the presence of metallic silver cubic phase (JCPDS04-0783) in the sample [37]. There are no characteristic peaks of impurity phases are observed from the patterns such as silver oxide phases (Ag_2O). Besides, there is no remarkable shift in the peak position for Ag/ZnO (3%) sample which indicates the positioning of silver particles on the surfaces of ZnO nanoparticles [38]. The crystallite size (D, Å) of the Ag/ZnO samples was determined by the Scherrer's formula (Eq. 3) [39]:

$$D = K\lambda\beta \cos \theta_B \tag{3}$$

Where, λ is the X-ray wavelength (1.54 Å), β is the angular width of the peak at half of its maximum intensity (full-width at half-maximum) corrected for the instrumental broadening, θ_B is the maximum of the Bragg diffraction peak and K is Scherrer constant (0.9Å). The average crystallite size of Ag/ZnO (3%) sample was calculated from the first seven peaks where it was 13.25 nm.
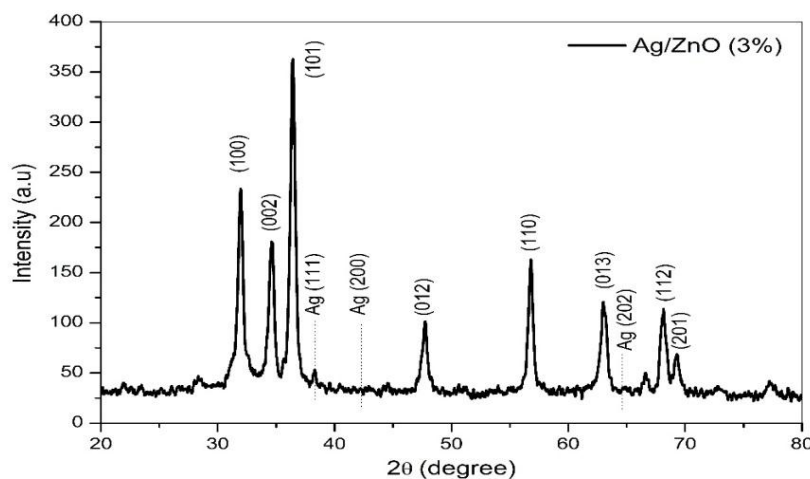
Figure 2: XRD patterns of pure ZnO and Ag/ZnO (3%) photocatalysts.

### 3.3. Scanning electron microscope (SEM) analysis

In order to investigate the surface morphology, size, shape and growth mechanism of Ag/ZnO (3%) nanoparticles, SEM analysis was performed (Figure 3). This image show some enhancement in the porosity and reduction in the density as a result of liberation of gases which creates the surface pores and holes [40]. The particle size was noted to nearly 28 nm for Ag/ZnO (3%) nanoparticles. When the concentration of added Ag increases the particles gets agglomerated and particle size increases heterogeneously for doped ZnO nanoparticles. Further increase of Ag content induces local aggregation of Ag particles [41].
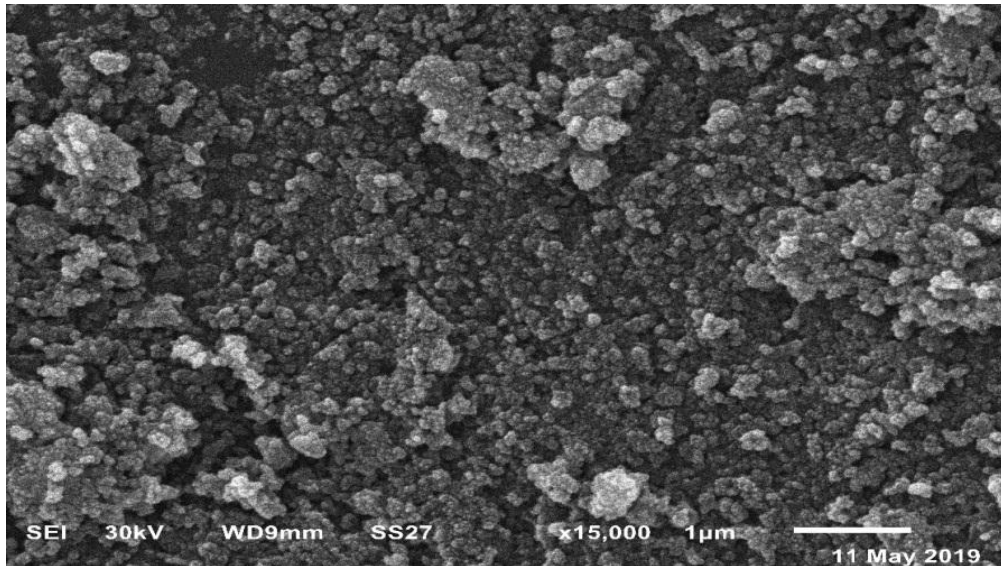
Figure 3: SEM image of Ag/ZnO (3%).\

3.4. Energy dispersive X-ray (EDX) analysis

The evaluation using energy dispersive X-ray analysis is based on the concept of providing unique set of peaks on X-ray spectrum for each element in unique atomic structure. The elemental composition of Ag/ZnO (3%) nanostructure was estimated by EDX analysis coupled with SEM. In the Ag/ZnO (3%) diagram shows the peaks of Ag, Zn and O (Figure 4). Zinc signals at 1.01, 8.69 and 9.53 keV, a peak for silver at 3.00 keV and oxygen peak at 0.53 keV were observed.
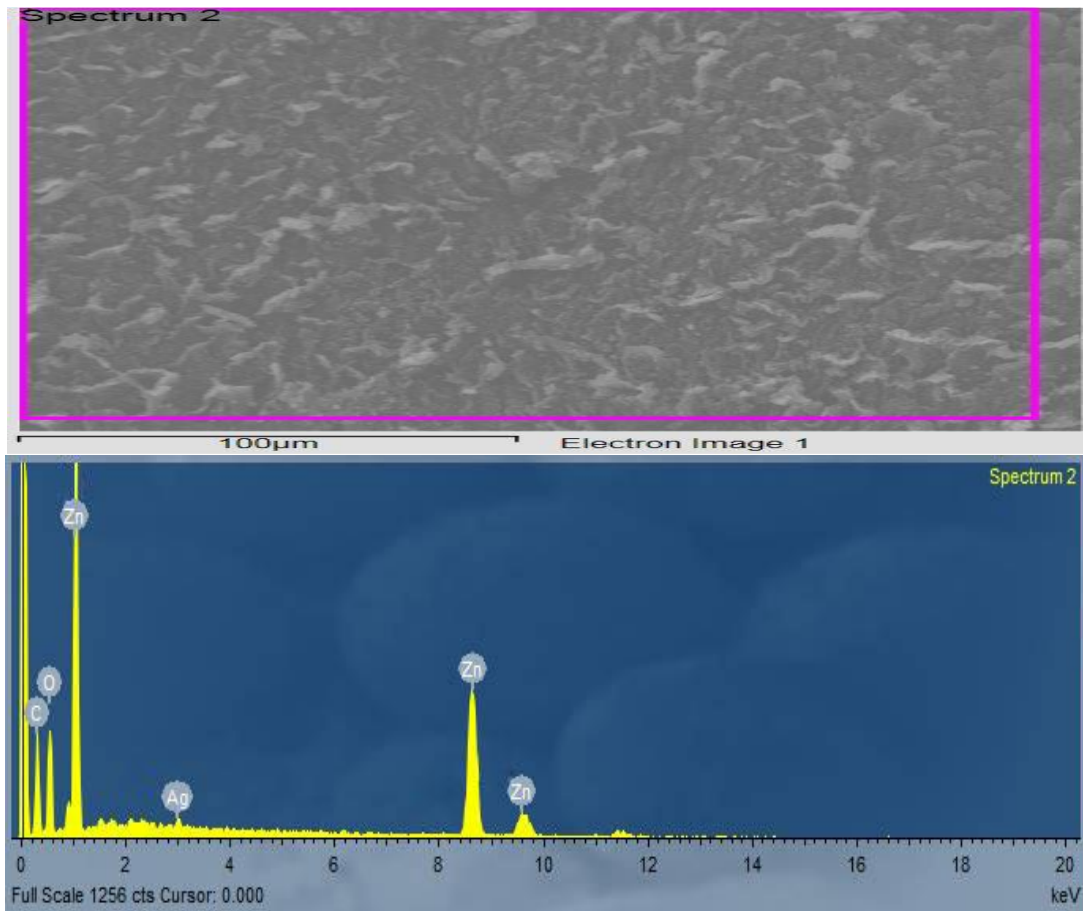
Figure 4: EDX spectrum of Ag/ZnO (3%).

3.5. Optical band gap energy (Eg)

The quantity of the energy band gap of Ag-ZnO (3%) nanostructure has been determined by studying of the optical properties of these particles using UV-visible spectroscopy. The band gap energy was determined using Tauc's formula which shows the relationship among absorption coefficient as follows (Eq. 4):

$$(\alpha h \upsilon)^{1/n} = B(h\upsilon - E_g) \qquad (4)$$

Where α is the absorption coefficient, h is Planck's constant and υ is the frequency ($\upsilon = c/\lambda$, λ is the wavelength, c is the light speed) [42]. Exponent n depends on the type of transition and it may have values 1/2, 2, 3/2 and 3 corresponding to the allowed direct, allowed indirect, forbidden direct and forbidden indirect transitions, respectively [43]. B is a constant and generally called band tailing parameter. Thus, the band gap energy was obtained graphically from $(\alpha h \upsilon)^2$ vs. $h\upsilon$ for direct transition, extrapolating the linear part on the abscissa according to Eq. 4. The band gap energy of Ag/ZnO was found to be 3.14 eV at 395 nm [44]. The narrowed band gap was proportional to photo excited electrons from the valence band into the conduction band, thus improving the optical property of pure and modified Ag/ZnO during the visible light region [45].

3.6. Brunauer-Emmett-Teller (BET) surface area

Because the reactions take place on the material surface, surface area is an important factor governing the catalytic activity of materials. In general, catalytic activity increases with increasing the surface area. The Brunauer-Emmett-Teller (BET) [46] surface area and Barrett-Joyner-Halenda (BJH) pore size of Ag/ZnO (3%) have been estimated using N_2 adsorption/desorption measurements at 77 K (Figure 5). The N_2 adsorption-desorption isotherms of Ag/ZnO (3%) nanoparticles are assorted as type II that pointed to non-porous solid at P/P_o = 0.99. The isotherm is completely reversible without any hysteresis loop enlightening the absence of any pore type which could allow capillary condensation process. This type of isotherm is the characteristic property of microporous structures. The specific surface area was calculated by BET equation in its normal range of applicability and adopting a value of 16.2 Å for the cross-section area of N_2 molecule and it was found to be 16.855 m²/g for Ag/ZnO (3%). However, the total pore volume at saturation pressure and expressed as liquid volume were found 0.157 cm³/g for Ag/ZnO (3%). As well as the pore radii were calculated by BJH pore size distribution curve and were found to be 1.847 nm for Ag/ZnO (3%) [47].
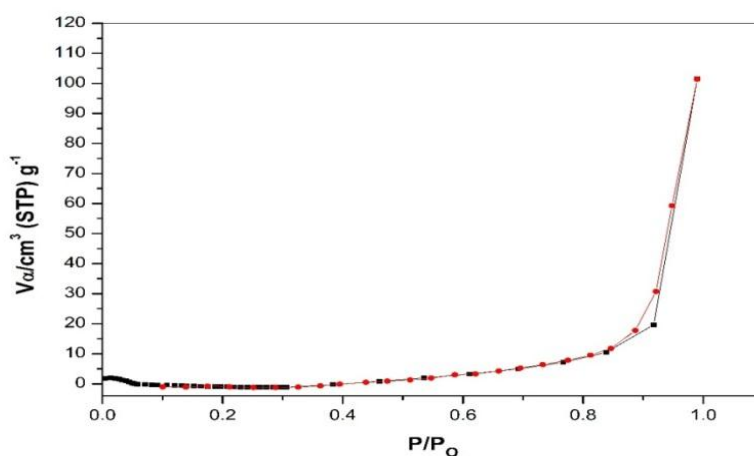

Figure 5: Sorption isotherm of Ag/ZnO (3%) collected by N_2 adsorption/desorption experiment at 77 K.

3.7. Determination of point of zero charge (pHPZC)

Surface charge of Ag/ZnO (3%) was determined by the PZC, which is defined as the pH (pHPZC) at which the positive charges on the surface equal the negative charges [48]. The pHPZC of Ag/ZnO (3%) was found to be 7.6. This shows that below this pH, the Ag/ZnO (3%) acquires a positive charge owing to protonation of functional groups and above this pH, negative charge exists on the surface.

3.8. Effect of Ag loading on the photocatalytic activity

The photocatalytic activity of Ag/ZnO can further increase with the increasing Ag content from 1 to 3%. However, a further increase in Ag content (3-9%) leads to a reduction of the photocatalytic activity. Figure 6 indicates that the highest photocatalytic activity can be obtained for Ag/ZnO with the optimal Ag content (3%). Excessive coverage o ZnO catalyst with Ag limits the amount of UV irradiation reaching to the ZnO surface, reducing the number of photogenerated e− – h+ pairs and consequently, lowering the ZnO photoactivity.
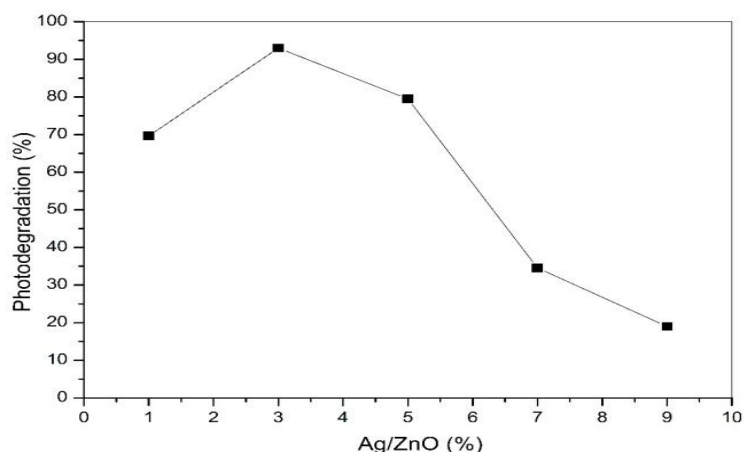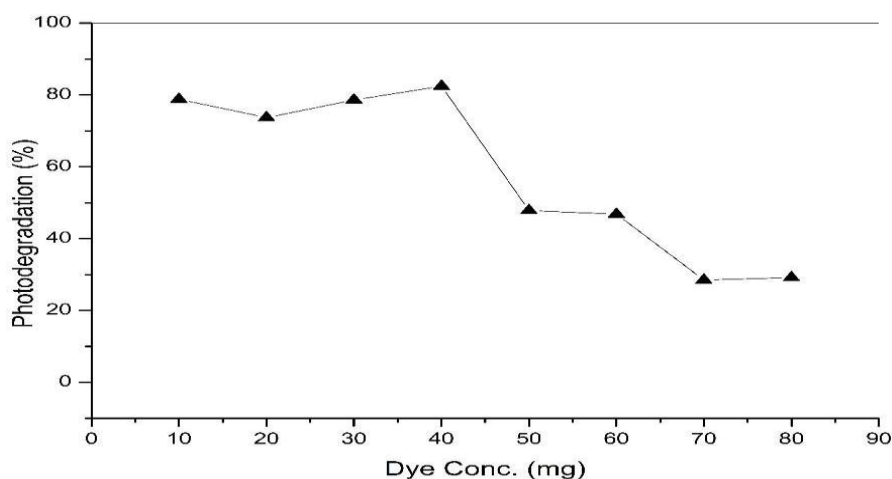
Figure 6: Effect of Ag content on the photodegradation activity of ZnO photocatalysts (initial dye concentration 40 mg/L, dosage 1.0 g/L and pH = 7) under UV irradiation time for 30 min.

3.9. Effect of Operating Parameters on the Photocatalytic degradation of RB21
3.9.1. Effect of initial dye concentration

The influence of preliminary dye concentration on its degradation has been studied with different concentrations of RB21 from 10 to 80 mg/L with a constant concentration of Ag/ZnO (3%) catalyst at 0.6 g/L. Results summary for both catalysts on degradation rates of RB21 after reaction time of 30 min. are shown in (Figure 7). It is generally noted that the degradation rate of low initial concentrations of RB21 (up to 40 mg/L) is more than that of the higher initial concentrations [49]. Accordingly, to enhance the removal efficiency of dye, lower initial concentration of the dye could be used [50]. The rate of degradation depends on the probability of evolution of $^{\bullet}$OH radicals on the catalyst surface and on the probability of reacting these $^{\bullet}$OH radicals with RB21 molecules. As a result, it is expected that increasing the initial concentration of RB21 will increase the probability of reaction between RB21 molecules and oxidizing species which will lead to an improvement in the degradation rate. Contrarily, as the initial concentration of RB21 dye increases, the degradation efficiency of RB21 decreases [51].

Figure 7: Effect of initial dye concentration on the photodegradation activity of Ag/ZnO (3%) photocatalysts (dosage 1.0 g/L and pH = 7) under UV irradiation time for 30 min.
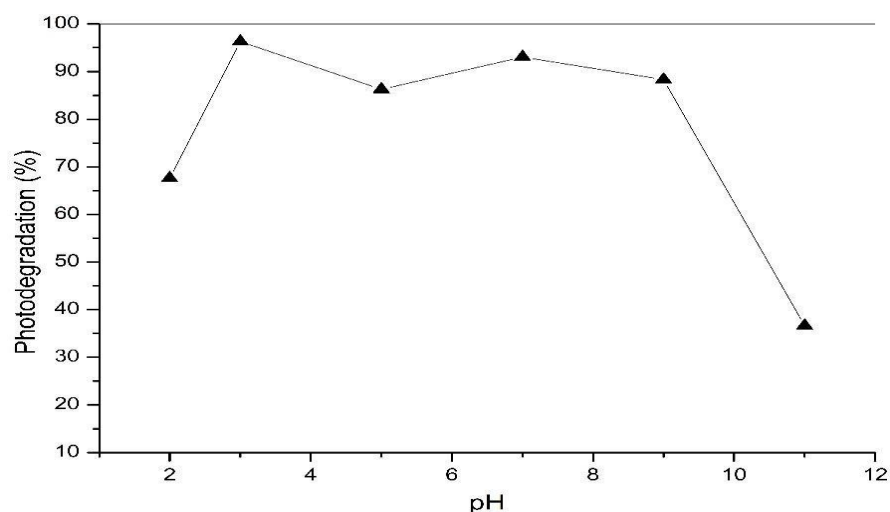
3.9.2. Effect of photocatalyt dosage

The effect of the catalyst concentration on the photodegradation efficiency of the process was estimated in the range of 0.2–1.8 g/L keeping RB21 dye concentration constant at 40 mg/L. The photodegradation rate of RB21 grows up with increasing the photocatalyst dosage (to the optimum value 1.0 g/L for Ag/ZnO (3%) and then goes down. The more the photocatalyst amount, the more the active sites are found on the photocatalyst surface, which leads to promotion of hydroxyl radical formation [52]. However, over increase in the amount of the catalyst has a negative effect, because of the screening effect of the aggregation of catalyst particles which can prevent photons to get to inner surface of the catalyst [53]. As well as, an excess amount of the catalyst reduces

the light penetration through shielding effect that of the suspended particles and as a result reduces photodegradation rate [54].

3.9.3. *Effect of pH*

The photocatalytic activity is highly affected by the material surface charge properties, the molecule charge, the adsorption of the organic molecule on the photocatalyst surface and the amount of hydroxyl radicals [52,53]. The effect of changing pH from 2 to 11 for the initial RB21 solution is shown in Figure 8, for an initial RB21 concentration of 40 mg/L, over Ag/ZnO (3%) photoctalysts (1.0 g/L), and under UV irradiation. Photocatalytic degradation efficiency decreases with a further raise in pH, showing that the initial pH of the dye solution affects the adsorption of the organic compound on the photocatalyst surface [54].

Dye photodegradation and thus adsorption seem to be chosen at pH around the zero point charge pH (pHzpc). At a pH higher than 8 the surface of ZnO photocatalyst is negatively charged, whereas at pH lower than 8 it converts positively charged. Because the type of RB21 is anionic dye, a pH less than that corresponding to the zero point charge prefers the adsorption of RB21 molecule on the catalyst surface which results in an enhanced degradation of RB21 under neutral and acidic conditions.

Figure 8: Effect of pH on the properties of Ag/ZnO (3%) photocatalysts
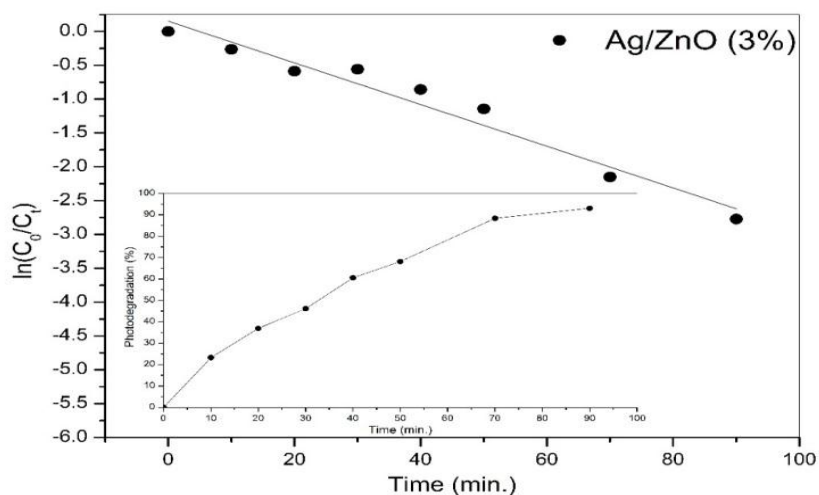(40 g/L dye concentration and dosage 1.0 g/L) under UV irradiation time for 30 min.

3.10. *Estimation of chemical oxygen demand (COD)*

To measure the organic strength of wastewater, the chemical oxygen demand (COD) is widely used as an effective technique [55]. The test allowed the measurement of waste in terms of the total quantity of oxygen required for oxidation of organic matter to CO_2 and H_2O. Chemical oxygen demand (COD) was used to examine the photodecolorization of the dye [56]. The COD of the dye solution before and after the treatment was estimated. Chemical oxygen demand was measured after exposure the sample to UV irradiations at times 0, 30, 60 min to check the photodecolorization of RB21 dye and found to be 210, 105, 50 ppm, respectively. The observed decrease in the COD values of the preserved dye solution with increasing time indicating the complete mineralization of dye into non-toxic species.

3.11. *Degradation Kinetics*

The photodegradation rate of RB21 dye on 1.0 g/L of Ag/ZnO (3%) photocatalysts was evaluated under UV irradiation (Figure 9). Generally, photocatalytic processes are performed only in water because the radicals can only react with the dye dissociated. A pseudo-first-order kinetics equation was used to estimate the kinetic rate constant (k) value for the photodegradation process of RB21 onto the photocatalysts surface and are expressed using Eq. (2). The kinetic constant was determined by the analytical integration method. The linear relationship between $\ln(C_0/C_t)$ and the reaction time *t* of RB21 dye follows a pseudo-first-order kinetics functioning with correlation coefficient ($R^2 = 0.9854$) for Ag/ZnO (3%) [56]. The photocatalytic activity of Ag/ZnO can further increase with the increasing Ag content from 1 to 3%. However, a further increase in Ag content (3-9%) leads to a reduction of the photocatalytic activity. The above results indicate that the highest photocatalytic activity can be obtained for Ag/ZnO with the optimal Ag content (3%), and provided that the photocatalytic reaction follows a pseudo-first-order reaction, the corresponding apparent rate constant (k) is estimated to be ca. 3.07×10^{-2} min^{-1} (Figure 9) [57].

Figure 9: Photocatalytic degradation kinetic curves of RB21 over Ag/ZnO (3%) under UV irradiation (40 mg/L dye concentration, dosage 1.0 g/L and pH = 7).

3.12. Stability of Photocatalyst ZnO

The practical applications for the photocatalysts required excellent properties such as the maintaining of recyclability and high photocatalytic activity. So that, the stability of the prepared photocatalysts Ag/ZnO (3%) was investigated by recycling experiments of the photocatalytic degradation of RB21 in the presence of UV irradiation. In this experiment, the photocatalyst was separated from the sample and collected after each cycle by centrifugation, then washed with both distilled water and ethanol and dried in an oven at 100 °C. The sample was then reused for subsequent degradation. As can be seen, the efficiency of the degradation of RB21 after 90 min decreased from 93.04 to 88.87 after three cycles for Ag/ZnO (3%), respectively. Also, the photocatalytic activity of the samples only minimally decreases, due to the unavoidable loss of photocatalysts during the cycle processes.

3.13. Mechanism of Photodegradation

The factors such as band gap energy, oxidation state of the dopant, and recombination of the photo-generated electron–hole pairs may be taken in the consideration for the improved photocatalytic properties of doped ZnO [58]. In general, the mechanism of photocatalytic degradation occurs by two main steps. The first one is to adsorb the pollutants molecules on the surface of photocatalysts and the seconded is the degradation of these pollutants. For this reason, the mechanism of the photocatalytic degradation of RB21 over the catalyst nanoparticles was proposed. At first, the RB21 molecules are adsorbed onto the imprinted layer of the catalyst to form a moderately stable complex. When the photocatalyst nanoparticles are illuminated under the excitation of UV light, Ag/ZnO nanoparticles can absorb light and generate electron/hole pairs.

To understand the mechanism of the degradation of RB21 on Ag/ZnO, it is important to indicate which of these reactive species plays the essential role the photocatalytic degradation process. The photodegradation of RB21 over Ag/ZnO was studied using silver nitrate (e− scavenger), potassium iodide (h+ scavenger) and isopropanol (OH$^{\bullet}$ scavenger) in the reaction solution [59].

When silver nitrate is added, a slightly changed in the photocatalytic degradation of RB21 dye is occurred. However, the removal rate are considerably decreased with the addition of a scavenger for OH$^{\bullet}$ (iso-propanol) and h^{+} (potassium iodide) [60]. Consequently, the holes and hydroxyl radicals are the main reactive species for the photocatalytic degradation of RB21 (Figure 9).

When the photocatalyst (ZnO) is irradiated with photons (hυ) of energy equal to or more than its band gap energy (3.36 eV), some electrons (e^{-}) of the valence band (VB) are excited and jump to the conduction band (CB) which leaves behind equivalent holes (h^{+}) in the VB:

$$ZnO + h\upsilon \quad \rightarrow \quad ZnO\ (h^{+}_{(VB)})\ +\ ZnO\ (e^{-}_{(CB)}) \hspace{2cm} (5)$$
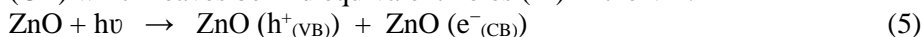
Where hυ is the energy required to transfer an electron from valence band to conduction band. In this photoexcited state, electrons can reduce dissolving oxygen to generate superoxide radical anions (O$_2^{\bullet-}$), whereas the photoexcited holes in VB have the ability to oxidize hydroxyl anions (OH^{-}) and H$_2$O to produce hydroxyl radicals

(OH$^\bullet$). After the formation these highly active radicals, they can destroy dye molecules and generate the small molecules CO_2 and H_2O [61].

$$e^-_{(CB)} + O_2 \rightarrow O_2^{\bullet-} \tag{6}$$
$$O_2^{\bullet-} + H_2O \rightarrow HO_2^{\bullet} + OH^{\bullet} \tag{7}$$

At the same time, the photoinduced holes could be trapped by the hydroxyl groups (or H_2O) on the photocatalyst surface to produce hydroxyl radicals (OH$^\bullet$) [62]:

$$OH^- + h^+_{(VB)} \rightarrow OH^{\bullet} \tag{8}$$
$$H_2O \leftrightarrow (H^+ + OH^-) + h^+_{(VB)} \rightarrow OH^{\bullet} + H^+ \tag{9}$$
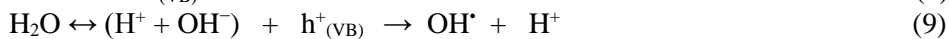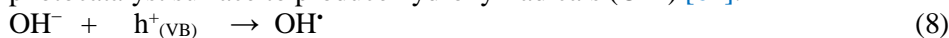
At the final stage, these highly active radicals have the ability to degrade the dye molecules (RB21) to yield carbon dioxide and water as follows:

$$OH^{\bullet} + RB21 + O_2 \rightarrow \text{products (}CO_2 \text{ and } H_2O\text{)} \tag{10}$$
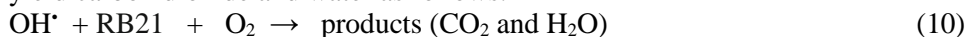
In the meantime, these photoinduced holes and electrons can recombine to lessen the efficiency of photodegradation. However, the addition of noble metals to the semiconductor photocatalyst can inhibit this recombination [63,64]:

$$ZnO\ (h^+_{(VB)}) + ZnO\ (e^-_{(CB)}) \rightarrow ZnO \tag{11}$$

By introducing silver atoms to the surface of ZnO, a metal-semiconductor Schottky barrier is created as a result of the low Fermi level of ZnO (F_{ZnO}) comparing to metallic Ag (F_{Ag}). This process is accompanying by the transfer of electrons from F_{Ag} to F_{ZnO}, until the two levels reach equilibrium and construct the new Fermi energy level of Ag/ZnO ($F_{Ag/ZnO}$). It promotes the transfer of photoexcited electrons from the conduction band of ZnO to Ag nanoparticles, while the holes still stay on the semiconductor surface. Besides, Ag nanoparticles can absorb more photons with energy greater than or equal to ZnO band gap which can further enhance the charge separation in ZnO. In this situation, more electrons are promoted from valence band to conduction band, forming corresponding holes in the valence band followed by an electron transfer from ZnO to Ag nanoparticles. So that, Ag nanoparticles perform as a sink for photo-generated electrons and play a fundamental role in banning electron-hole recombination [65,66]. The enhancing effect of Ag on the photocatalytic activity could be accounted for its ability to trap electrons, which reduces the recombination of electrons on Ag and holes on the ZnO by producing more OH$^\bullet$ [66]. In addition, Ag increases the life time of the photoinduced charge carriers [67,68].

$$Ag^+ + e^-_{(CB)} \rightarrow Ag \tag{12}$$
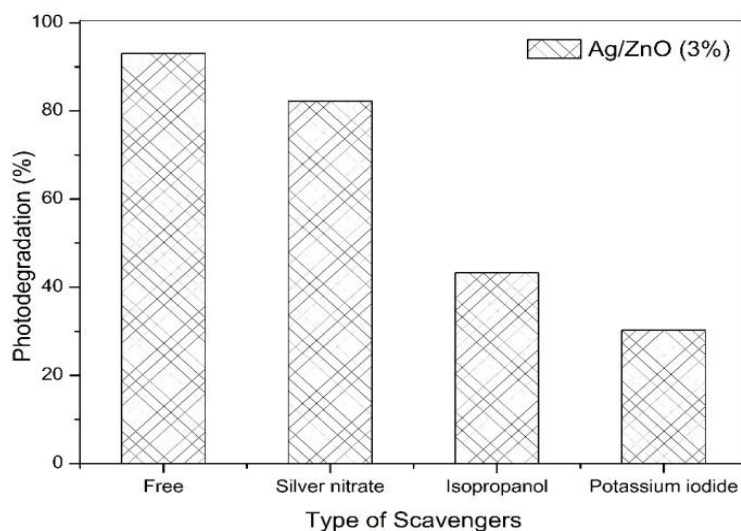
Fig. 10. Photodegradation ratio of RB21 over ZnO and Ag/ZnO (3%) in the absence and presence of various scavengers (potassium iodide, isopropanol and silver nitrate) under UV irradiation for 90 min (40 mg/L dye concentration, dosage 1.0 g/L and pH = 7).

Creation of OH$^\bullet$ free radicals is established by means of photoluminescence studies using terephthalic Acid (TPA) as a probe molecule. TPA reacts with OH$^\bullet$ free radicals to yield 2-hydroxyterphthalic acid which shows a characteristic luminescence peak at 420 nm [69]. The intense luminescence peak at 420 nm for sample containing Ag/ZnO + TPA after irradiation for 20, 40, 60, 80 and 100 min clearly shows the presence of OH$^\bullet$ free radicals during irradiation (Figure 10).
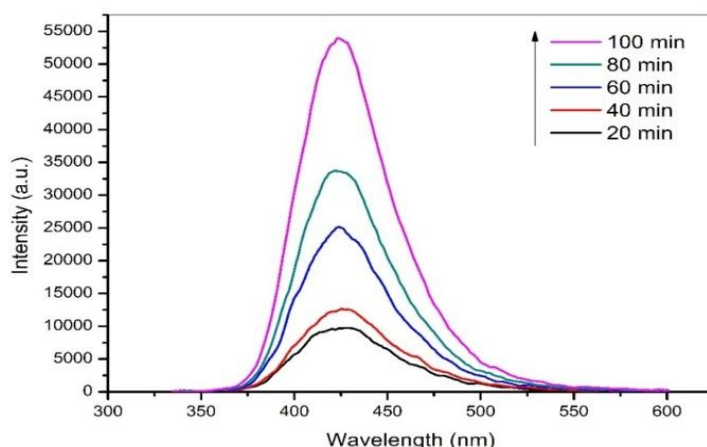
Figure 10: Photoluminescence spectra of Ag/ZnO (3%) + TPA after irradiation (40 mg/L initial dye concentration, 1.0 g/L Ag/ZnO, 4.8×10^{-4} M terephthalic acid and pH = 7) with the excitation wavelength of 315 nm.

Conclusion

In this work the photocatalytic activity of Ag/ZnO (3%) photocatalyst was examined for the treatment of aqueous solutions containing RB21 under UV light irradiation. The catalysts were characterized by different spectroscopic techniques. Ag/ZnO (3%) having higher surface area, and maximum Ag nanoparticle loading with surface area of 16.855 m^2/g. Optical measurements indicated a red shift in the absorption band edge after Ag doping. The band gap value of Ag/ZnO (3%) was found to be 3.14 eV. The effect of operation parameters such as pH, catalyst dosage, and initial dye concentration was estimated. It was found that the degradation of RB21 fitted the first-order kinetics and OH$^\bullet$ radicals were the main species. Formation of OH$^\bullet$ free radicals during irradiation is ascertained by photoluminescence studies using terephthalic acid as probe molecule. The degradation extent was checked by UV-vis spectroscopy and confirmed by chemical oxygen demand. Ag/ZnO (3%) showed the highest photocatalytic activity with a k value of 3.07×10^{-2} min^{-1}.

References

1. A. Paz, J. Carballo, M.J. Pérez, J.M. Domínguez, Biological treatment of model dyes and textile wastewaters, *Chemosphere*, 181 (2017) 168–177. doi:10.1016/j.chemosphere.2017.04.046.
2. L. Anju Chanu, W. Joychandra Singh, K. Jugeshwar Singh, K. Nomita Devi, Effect of operational parameters on the photocatalytic degradation of Methylene blue dye solution using manganese doped ZnO nanoparticles, *Results Phys.*, 12 (2019) 1230–1237. doi:10.1016/j.rinp.2018.12.089.
3. M. Samadi, M. Zirak, A. Naseri, M. Kheirabadi, M. Ebrahimi, A.Z. Moshfegh, Design and tailoring of one-dimensional ZnO nanomaterials for photocatalytic degradation of organic dyes: a review, Springer Netherlands, 2019. doi:10.1007/s11164-018-03729-5.
4. M. Punzi, A. Anbalagan, R. Aragão Börner, B.-M. Svensson, M. Jonstrup, B. Mattiasson, Degradation of a textile azo dye using biological treatment followed by photo-Fenton oxidation: Evaluation of toxicity and microbial community structure, *Chem. Eng. J.*, 270 (2015) 290–299. doi:10.1016/J.CEJ.2015.02.042.
5. R. Darvishi Cheshmeh Soltani, M. Safari, M. Mashayekhi, Sonocatalyzed decolorization of synthetic textile wastewater using sonochemically synthesized MgO nanostructures, *Ultrason. Sonochem.*, 30 (2016) 123–131. doi:10.1016/J.ULTSONCH.2015.11.018.
6. M. Pirhashemi, A. Habibi-Yangjeh, Ultrasonic-assisted preparation of plasmonic ZnO/Ag/Ag2WO4 nanocomposites with high visible-light photocatalytic performance for degradation of organic pollutants, *J. Colloid Interface Sci.*, 491 (2017) 216–229. doi:10.1016/J.JCIS.2016.12.044.
7. C.S.D. Rodrigues, L.M. Madeira, R.A.R. Boaventura, Treatment of textile dye wastewaters using ferrous sulphate in a chemical coagulation/flocculation process, *Environ. Technol.*, 34 (2013) 719–729. doi:10.1080/09593330.2012.715679.
8. S. Jorfi, R. Darvishi Cheshmeh Soltani, M. Ahmadi, A. Khataee, M. Safari, Sono-assisted adsorption of a textile dye on milk vetch-derived charcoal supported by silica nanopowder, *J. Environ. Manage.*, 187 (2017) 111–121. doi:10.1016/J.JENVMAN.2016.11.042.
9. M. Mousavi, A. Habibi-Yangjeh, S.R. Pouran, Review on magnetically separable graphitic carbon nitride-

based nanocomposites as promising visible-light-driven photocatalysts, *J. Mater. Sci. Mater.*, Electron. 29 (2018) 1719–1747. doi:10.1007/s10854-017-8166-x.

10. U.G. Akpan, B.H. Hameed, Parameters affecting the photocatalytic degradation of dyes using TiO2-based photocatalysts: A review, *J. Hazard. Mater.*, 170 (2009) 520–529. doi:10.1016/J.JHAZMAT.2009.05.039.

11. P. Singh, K. Mondal, A. Sharma, Reusable electrospun mesoporous ZnO nanofiber mats for photocatalytic degradation of polycyclic aromatic hydrocarbon dyes in wastewater, *J. Colloid Interface Sci.*, 394 (2013) 208–215. doi:10.1016/J.JCIS.2012.12.006.

12. K. Singh, S. Arora, Removal of Synthetic Textile Dyes From Wastewaters: A Critical Review on Present Treatment Technologies, *Crit. Rev. Environ. Sci. Technol.*, 41 (2011) 807–878. doi:10.1080/10643380903218376.

13. N. Liu, N. Lu, Y. Su, P. Wang, X. Quan, Fabrication of g-C3N4/Ti3C2 composite and its visible-light photocatalytic capability for ciprofloxacin degradation, *Sep. Purif. Technol.*, 211 (2019) 782–789. doi:10.1016/J.SEPPUR.2018.10.027.

14. H. Dong, G. Zeng, L. Tang, C. Fan, C. Zhang, X. He, Y. He, An overview on limitations of TiO2-based particles for photocatalytic degradation of organic pollutants and the corresponding countermeasures, *Water Res.*, 79 (2015) 128–146. doi:10.1016/J.WATRES.2015.04.038.

15. R.J. Tayade, P.K. Surolia, R.G. Kulkarni, R. V. Jasra, Photocatalytic degradation of dyes and organic contaminants in water using nanocrystalline anatase and rutile TiO$_2$, *Sci. Technol. Adv. Mater.*, 8 (2007) 455–462. doi:10.1016/j.stam.2007.05.006.

16. A. Mills, S.-K. Lee, A web-based overview of semiconductor photochemistry-based current commercial applications, *J. Photochem. Photobiol. A Chem.*, 152(2002)233–247. doi:10.1016/S1010-6030(02)00243-5.

17. C. Tian, Q. Zhang, A. Wu, M. Jiang, Z. Liang, B. Jiang, H. Fu, Cost-effective large-scale synthesis of ZnO photocatalyst with excellent performance for dye photodegradation, *Chem. Commun.*, 48 (2012) 2858. doi:10.1039/c2cc16434e.

18. C. Karunakaran, R. Dhanalakshmi, P. Gomathisankar, G. Manikandan, Enhanced phenol-photodegradation by particulate semiconductor mixtures: Interparticle electron-jump, *J. Hazard. Mater.*, 176 (2010) 799–806. doi:10.1016/J.JHAZMAT.2009.11.105.

19. A. Moezzi, A.M. McDonagh, M.B. Cortie, Zinc oxide particles: Synthesis, properties and applications, *Chem. Eng. J.*, 185–186 (2012) 1–22. doi:10.1016/J.CEJ.2012.01.076.

20. A. Anukaliani, M. Nirmala, M.G. Nair, K. Rekha, S.K. Samdarshi, R.G. Nair, Photocatalytic Activity of ZnO Nanopowders Synthesized by DC Thermal Plasma, *African J. Basic Appl. Sci.*, 2 (2010) 161–166. https://pdfs.semanticscholar.org/a5fb/675e3305fbf423d6fc04cd828441bf92ceaf.pdf .

21. M. Sleiman, D. Vildozo, C. Ferronato, J.-M. Chovelon, Photocatalytic degradation of azo dye Metanil Yellow: Optimization and kinetic modeling using a chemometric approach, *Appl. Catal. B Environ.*, 77 (2007) 1–11. doi:10.1016/J.APCATB.2007.06.015.

22. N.F. Djaja, R. Saleh, N.F. Djaja, R. Saleh, Characteristics and Photocatalytics Activities of Ce-Doped ZnO Nanoparticles, *Mater. Sci. Appl.*, 04 (2013) 145–152. doi:10.4236/msa.2013.42017.

23. J. Bandara, H. Weerasinghe, Solid-state dye-sensitized solar cell with p-type NiO as a hole collector, *Sol. Energy Mater. Sol. Cells.*, 85 (2005) 385–390. doi:10.1016/J.SOLMAT.2004.05.010.

24. R.M. Mohamed, A. Shawky, CNT supported Mn-doped ZnO nanoparticles: simple synthesis and improved photocatalytic activity for degradation of malachite green dye under visible light, *Appl. Nanosci.*, 8 (2018) 1179–1188. doi:10.1007/s13204-018-0742-8.

25. M. Ahmad, E. Ahmed, Y. Zhang, N.R. Khalid, J. Xu, M. Ullah, Z. Hong, Preparation of highly efficient Al-doped ZnO photocatalyst by combustion synthesis, *Curr. Appl. Phys.*, 13 (2013) 697–704. doi:10.1016/J.CAP.2012.11.008.

26. T.N.N. Ravishankar, K. Manjunatha, T. Ramakrishnappa, G. Nagaraju, D. Kumar, S. Sarakar, B.S.S. Anandakumar, G.T.T. Chandrappa, V. Reddy, J. Dupont, Comparison of the photocatalytic degradation of trypan blue by undoped and silver-doped zinc oxide nanoparticles, *Mater. Sci. Semicond. Process.*, 26 (2014) 7–17. doi:10.1016/j.mssp.2014.03.027.

27. Chuncheng Chen, Pengxiang Lei, Hongwei Ji, and Wanhong Ma, J. Zhao*, H. Hidaka, N. Serpone, Photocatalysis by Titanium Dioxide and Polyoxometalate/TiO$_2$ Cocatalysts. *Intermediates and Mechanistic Study*, (2003). doi:10.1021/ES034384F.

28. W. Xie, Y. Li, W. Sun, J. Huang, H. Xie, X. Zhao, Surface modification of ZnO with Ag improves its photocatalytic efficiency and photostability, *J. Photochem. Photobiol. A Chem.*, 216 (2010) 149–155. doi:10.1016/J.JPHOTOCHEM.2010.06.032.

29. R. Shirley, The CRYSFIRE System for Automatic Powder Indexing: User's Manual, (2002).

30. K.Z. Elwakeel, A.A. El-Bindary, E.Y. Kouta, E. Guibal, Functionalization of polyacrylonitrile/Na-Y-zeolite composite with amidoxime groups for the sorption of Cu(II), Cd(II) and Pb(II) metal ions, *Chem. Eng. J*., 332 (2018) 727–736. doi:10.1016/J.CEJ.2017.09.091.

31. H.A. Kiwaan, T.M. Atwee, E.A. Azab, A.A. El-Bindary, Efficient photocatalytic degradation of Acid Red 57 using synthesized ZnO nanowires, *J. Chinese Chem. Soc*., 66 (2019) 89–98. doi:10.1002/jccs.201800092.

32. A.R. Prasad, P. Rugmini Ammal, A. Joseph, Effective photocatalytic removal of different dye stuffs using green synthesized zinc oxide nanogranules, *Mater. Res. Bull*., 102 (2018) 116–121. doi:10.1016/J.MATERRESBULL.2018.02.022.

33. K. Saoud, R. Alsoubaihi, N. Bensalah, T. Bora, M. Bertino, J. Dutta, Synthesis of supported silver nano-spheres on zinc oxide nanorods for visible light photocatalytic applications, *Mater. Res. Bull*., 63 (2015) 134–140. doi:10.1016/J.MATERRESBULL.2014.12.001.

34. G. Xiong, U. Pal, J.G. Serrano, K.B. Ucer, R.T. Williams, Photoluminesence and FTIR study of ZnO nanoparticles: the impurity and defect perspective, *Phys. Status Solidi*., 3 (2006) 3577–3581. doi:10.1002/pssc.200672164.

35. K. Omri, I. Najeh, R. Dhahri, J. El Ghoul, L. El Mir, Effects of temperature on the optical and electrical properties of ZnO nanoparticles synthesized by sol–gel method, *Microelectron. Eng*., 128 (2014) 53–58. doi:10.1016/J.MEE.2014.05.029.

36. R. Krithiga, G. Chandrasekaran, Synthesis, strucutral and optical properties of vanadium doped zinc oxide nanograins, J. Cryst. Growth. 311 (2009) 4610–4614. doi:10.1016/J.JCRYSGRO.2009.08.033.

37. V.R. Chelli, A.K. Golder, Ag-doping on ZnO support mediated by bio-analytes rich in ascorbic acid for photocatalytic degradation of dipyrone drug, *Chemosphere*, 208 (2018) 149–158. doi:10.1016/J.CHEMOSPHERE.2018.05.158.

38. V. Vaiano, M. Matarangolo, J.J. Murcia, H. Rojas, J.A. Navío, M.C. Hidalgo, Enhanced photocatalytic removal of phenol from aqueous solutions using ZnO modified with Ag, *Appl. Catal. B Environ*., 225 (2018) 197–206. doi:10.1016/J.APCATB.2017.11.075.

39. A.L. Patterson, The Scherrer Formula for X-Ray Particle Size Determination, *Phys. Rev*., 56 (1939) 978–982. doi:10.1103/PhysRev.56.978.

40. S. Suwanboon, Structural and Optical Properties of Nanocrystalline ZnO Powder from Sol-Gel Method, (n.d.). doi:10.2306/scienceasia1513-1874.2008.34.031.

41. D. Lin, H. Wu, R. Zhang, W. Pan, Enhanced Photocatalysis of Electrospun Ag−ZnO Heterostructured Nanofibers, *Chem. Mater*., 21 (2009) 3479–3484. doi:10.1021/cm900225p.

42. J. Tauc, R. Grigorovici, A. Vancu, Optical Properties and Electronic Structure of Amorphous Germanium, *Phys. Status Solidi*, 15 (1966) 627–637. doi:10.1002/pssb.19660150224.

43. A.A. Essawy, Silver imprinted zinc oxide nanoparticles: Green synthetic approach, characterization and efficient sunlight-induced photocatalytic water detoxification, *J. Clean. Prod*., 183 (2018) 1011–1020. doi:10.1016/J.JCLEPRO.2018.02.214.

44. P. JI, Optical Process in Semiconductors, Prentice- Hall, New Jersey, 1971.

45. A.M.A. Abdelsamad, T.A. Gad-Allah, F.A. Mahmoud, M.I. Badawy, Enhanced photocatalytic degradation of textile wastewater using Ag/ZnO thin films, *J. Water Process Eng*., 25 (2018) 88–95. doi:10.1016/J.JWPE.2018.07.002.

46. S. Brunauer, P.H. Emmett, E. Teller, Adsorption of Gases in Multimolecular Layers, *J. Am. Chem. Soc*., 60 (1938) 309–319. doi:10.1021/ja01269a023.

47. D.E. Wurster, E. Oh, J.C. Wang, Determination of the mechanism for the decrease in zinc oxide surface area upon high-temperature drying., *J. Pharm. Sci*., 84 (1995) 1301–7. doi:10.1002/jps.2600841109.

48. S. Sadaf, H.N. Bhatti, M. Arif, M. Amin, F. Nazar, Adsorptive removal of direct dyes by PEI-treated peanut husk biomass: Box–Behnken experimental design, *Chem. Ecol*., 31 (2015) 252–264. doi:10.1080/02757540.2014.950568.

49. I.K. Konstantinou, T.A. Albanis, TiO2-assisted photocatalytic degradation of azo dyes in aqueous solution: kinetic and mechanistic investigations: A review, *Appl. Catal. B Environ*., 49 (2004) 1–14. doi:10.1016/J.APCATB.2003.11.010.

50. H.R. Pouretedal, A. Norozi, M.H. Keshavarz, A. Semnani, Nanoparticles of zinc sulfide doped with manganese, nickel and copper as nanophotocatalyst in the degradation of organic dyes, *J. Hazard. Mater*., 162 (2009) 674–681. doi:10.1016/J.JHAZMAT.2008.05.128.

51. A. Elaziouti, N. Laouedj, A. Bekka, Synergetic effects of Sr-doped CuBi2O4 catalyst with enhanced photoactivity under UVA– light irradiation, *Environ. Sci. Pollut. Res*., 23 (2016) 15862–15876. doi:10.1007/s11356-015-4946-0.

52. X.X. Wang, Z. Wu, Y. Wang, W. Wang, X.X. Wang, Y. Bu, J. Zhao, Adsorption–photodegradation of humic acid in water by using ZnO coupled TiO$_2$/bamboo charcoal under visible light irradiation, *J. Hazard. Mater*., 262 (2013) 16–24. doi:10.1016/J.JHAZMAT.2013.08.037.

53. A. Nezamzadeh-Ejhieh, E. Shahriari, Photocatalytic decolorization of methyl green using Fe(II)-o-phenanthroline as supported onto zeolite Y, *J. Ind. Eng. Chem*., 20 (2014) 2719–2726. doi:10.1016/J.JIEC.2013.10.060.

54. V. Kuzhalosai, B. Subash, A. Senthilraja, P. Dhatshanamurthi, M. Shanthi, Synthesis, characterization and photocatalytic properties of SnO2–ZnO composite under UV-A light, *Spectrochim. Acta Part A*, 115 (2013) 876–882. doi:10.1016/J.SAA.2013.06.106.

55. M.C. Hasegawa, J.F. de S. Daniel, K. Takashima, G.A. Batista, S.M.C.P. da Silva, COD removal and toxicity decrease from tannery wastewater by zinc oxide-assisted photocatalysis: a case study, *Environ. Technol*., 35 (2014) 1589–1595. doi:10.1080/09593330.2013.874499.

56. A. Pruna, Z. Wu, J.A. Zapien, Y.Y. Li, A. Ruotolo, Enhanced photocatalytic performance of ZnO nanostructures by electrochemical hybridization with graphene oxide, *Appl. Surf. Sci*., 441 (2018) 936–944. doi:10.1016/J.APSUSC.2018.02.117.

57. A.A. El-Bindary, S.M. El-Marsafy, A.A. El-Maddah, Enhancement of the photocatalytic activity of ZnO nanoparticles by silver doping for the degradation of AY99 contaminants, *J. Mol. Struct*., 1191 (2019) 76–84. doi:10.1016/j.molstruc.2019.04.064.

58. E. Topkaya, M. Konyar, H.C. Yatmaz, K. Öztürk, Pure ZnO and composite ZnO/TiO2 catalyst plates: A comparative study for the degradation of azo dye, pesticide and antibiotic in aqueous solutions, *J. Colloid Interface Sci*., 430 (2014) 6–11. doi:10.1016/J.JCIS.2014.05.022.

59. M. Chen, C. Bao, T. Cun, Q. Huang, One-pot synthesis of ZnO/oligoaniline nanocomposites with improved removal of organic dyes in water: Effect of adsorption on photocatalytic degradation, *Mater. Res. Bull*., 95 (2017) 459–467. doi:10.1016/j.materresbull.2017.08.017.

60. X. Chen, Z. Wu, D. Liu, Z. Gao, Preparation of ZnO Photocatalyst for the Efficient and Rapid Photocatalytic Degradation of Azo Dyes, *Nanoscale Res. Lett*., 12 (2017). doi:10.1186/s11671-017-1904-4.

61. A. Houas, H. Lachheb, M. Ksibi, E. Elaloui, C. Guillard, J.-M. Herrmann, Photocatalytic degradation pathway of methylene blue in water, *Appl. Catal. B Environ*., 31 (2001) 145–157. doi:10.1016/S0926-3373(00)00276-9.

62. L. Saikia, D. Bhuyan, M. Saikia, B. Malakar, D.K. Dutta, P. Sengupta, Photocatalytic performance of ZnO nanomaterials for self sensitized degradation of malachite green dye under solar light, *Appl. Catal. A Gen*., 490 (2015) 42–49. doi:10.1016/J.APCATA.2014.10.053.

63. H. Liu, Y. Hu, Z. Zhang, X. Liu, H. Jia, B. Xu, Synthesis of spherical Ag/ZnO heterostructural composites with excellent photocatalytic activity under visible light and UV irradiation, *Appl. Surf. Sci*., 355 (2015) 644–652. doi:10.1016/J.APSUSC.2015.07.012.

64. Y. Yang, H. Li, F. Hou, J. Hu, X. Zhang, Y. Wang, Facile synthesis of ZnO/Ag nanocomposites with enhanced photocatalytic properties under visible light, *Mater. Lett*., 180 (2016) 97–100. doi:10.1016/J.MATLET.2016.05.117.

65. S. Kuriakose, V. Choudhary, B. Satpati, S. Mohapatra, Facile synthesis of Ag–ZnO hybrid nanospindles for highly efficient photocatalytic degradation of methyl orange, *Phys. Chem. Chem. Phys*., 16 (2014) 17560. doi:10.1039/C4CP02228A.

66. K. Saoud, R. Al Soubaihi, S. Saeed, N. Bensalah, M. Al-Fandi, T. Singh, Heterogeneous Ag and ZnOBased Photocatalytic ForWaste Water Treatment Under Different Irradiation Conditions, *J. Mater. Environ. Sci*., 9 (2018) 400–413. doi:10.26872/jmes.2018.9.2.44.

67. M. Kheirabadi, M. Samadi, E. Asadian, Y. Zhou, C. Dong, J. Zhang, A.Z. Moshfegh, Well-designed Ag/ZnO/3D graphene structure for dye removal: Adsorption, photocatalysis and physical separation capabilities, *J. Colloid Interface Sci*., 537 (2019) 66–78. doi:10.1016/J.JCIS.2018.10.102.

68. R. R., S. K.S., G.K.G., ZnO:Ag nanorods as efficient photocatalysts: Sunlight driven photocatalytic degradation of sulforhodamine B, *Appl. Surf. Sci*., 427 (2018) 863–875. doi:10.1016/J.APSUSC.2017.09.050.

69. X.H. Lin, S.N. Lee, W. Zhang, S.F.Y. Li, Photocatalytic degradation of terephthalic acid on sulfated titania particles and identification of fluorescent intermediates, *J. Hazard. Mater*., 303 (2016) 64–75. doi:10.1016/J.JHAZMAT.2015.10.025.

(2019) ; http://www.jmaterenvironsci.com